# Parameter Identification for PV Modules Based on an Environment-Dependent Double-Diode Model

Fabricio Bradaschia, *Senior Member, IEEE*, Marcelo C. Cavalcanti, Aguinaldo José do Nascimento, Jr., Emerson Alves da Silva, and Gustavo Medeiros de Souza Azevedo, *Member, IEEE*

***Abstract*—Most of the photovoltaic (PV) models involve mainly the reproduction of the nonlinear *I–V* curves for PV modules with a certain degree of accuracy. Previous researches have used equivalent circuits based on common electronic devices to model the real behavior of PV modules, such as the single and double diode models. Unfortunately, those models are static, i.e., they can reproduce the *I–V* curve of a PV module for a specific environmental condition (fixed irradiance and temperature). As consequence, different models should be obtained for each different environmental condition, restricting the use of the models for a limited set of irradiance and temperature values. The first contribution of this paper is the proposition of an irradiance and temperature dependent double-diode model for PV modules. In this model, the internal parameters depend on the environmental conditions, extrapolating its use for temperature and irradiance values different from those the parameters were initially estimated. In addition, two parameter estimation techniques are proposed for this new model. The techniques use a combination of analytical equations and numerical optimization based on the pattern search algorithm. Comparison results based on experimental *I–V* curves of real PV modules are presented in order to prove the accuracy of the model and techniques.**

***Index Terms*—Parameter estimation, photovoltaic (PV) systems.**

## I. Introduction

In general, the determination and analysis of the characteristic *I–V* curve of a photovoltaic (PV) module is performed under certain specific conditions of temperature ($T$), irradiance ($S$), and air mass (AM). These criteria characterize the standard test condition (STC), where $T = 25\,^{\circ}\text{C}$, $S = 1000\,\text{W/m}^2$, and AM $= 1.5$. However, when a PV module is installed in a plant, it is more common to be subjected to conditions outside the STC. In this circumstance, important information provided by the manufacturers, such as open-circuit voltage ($V_{\text{oc}}$), short-circuit current ($I_{\text{sc}}$), and maximum power point (MPP) data ($P_{mp}$, $V_{mp}$, and $I_{mp}$) are no longer valid. Many of these data can be obtained experimentally, but there are other parameters that act simultaneously influencing the performance of the PV module, and they are generally not provided by the manufacturer. For those reasons, it is a difficult task developing precise models for PV modules, which are based on the understanding of the physics of a PV cell.

Developing suitable models to simulate and predict the behavior of PV modules is very important, especially when designing, manufacturing, and evaluating PV systems in a macroscale. The knowledge of the parameters of the model from *I–V* measurements is both useful for the set of cells and the simulation of the system, since they carry information about the physical properties and quality control of these solar generators [1]. However, most of the applications that use the PV model are intended to estimate the output power with the highest possible accuracy [2]. Therefore, it is more interesting to build a model based on power-to-voltage (*P–V*) measurements than one based on *I–V* measurements.

Currently, most of the models involve the reproduction of the nonlinear *I–V* curve of the PV module for a specific condition of temperature and irradiance. Previous researches have used equivalent circuits based on common electronic devices to model the real behavior of PV modules, such as the single and double diode models [3]. The simplest model [4] consists of a current source (representing the photogenerated current $I_g$) in parallel with a diode (representing the $p-n$ junction of the PV cell $d$). The diode has a current ($I_d$) which represents the diffusion mechanism that depends on the diode saturation current $I_0$ and ideality factor $A$. An improvement of the model can be done by adding a series resistance ($R_s$) to the equivalent circuit, representing the resistivity of the material and ohmic losses because of the electrical contacts [5]. This model is also known as four-parameter model or $R_s$ model [6]. More modifications can be made by adding a resistance in parallel with the current source, representing the parasitic currents present at the junction because of defects through the device. In this case, we have a five-parameter model, also known as the $R_p$ model or a full single-diode model. This model offers a good compromise between simplicity and precision, being able to behave as the $R_s$ model if $R_p$ tends to infinity [1].

Unfortunately, in real PV cells, the phenomenon of charge recombination represents a substantial current loss that cannot be adequately represented using the single-diode model [7], [8], since this simplified model is based on the assumption that the loss by recombination in the depletion region is absent. Thus, to describe the $p-n$ junction more accurately, a second diode

Manuscript received April 9, 2019; revised May 29, 2019; accepted June 7, 2019. Date of publication July 2, 2019; date of current version August 22, 2019. This work was supported in part by the Conselho Nacional de Desenvolvimento Científico e Tecnológico - CNPq, in part by the Coordenação de Aperfeiçoamento de Pessoal de Nível Superior - CAPES, and in part by the Fundação de Amparo à Ciência e Tecnologia do Estado de Pernambuco - Facepe, Brazil. *(Corresponding author: Marcelo C. Cavalcanti.)*

The authors are with the Department of Electrical Engineering, Federal University of Pernambuco, 50740-530 Recife, Brazil (e-mail: fabricio.bradaschia@ufpe.br; marcelo.ccavalcanti@ufpe.br; aguinaldojunior10@hotmail.com; emerson.silva90@gmail.com; gustavomsa@aim.com).

Digital Object Identifier 10.1109/JPHOTOV.2019.2923336

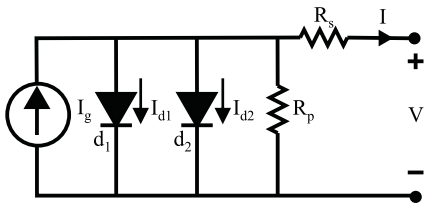


Fig. 1. Double-diode model of a PV module.

($d_2$) is added, leading to a more precise model, known as the double-diode model [3], [7], which is shown in Fig. 1. In this model, the diffusion current because of the majority charge carriers is represented by $I_{d1}$ and flows through the first diode ($d_1$), while the recombination current because of the minority charge carriers is represented by $I_{d2}$ and flows through the second diode ($d_2$) [1]. Since the second diode generates two more parameters, this model is also known as seven-parameter model.

In general, the analytical determination of the parameters of a PV model is a difficult task [9], primarily because of the nonlinearity observed in the transcendental equation of the $p-n$ junction. Another difficulty is that, in general, the parameters $I_g$, $R_s$, $R_p$, $I_{01}$, $I_{02}$, $A_1$, and $A_2$ are not fixed parameters, but dependent on $S$ and $T$ [1]. Because of this complexity, several different techniques for determining these parameters have been proposed in literature. Some techniques are based on analytical equations, numerical solutions, iterative or optimization algorithms to determine four [3], five [10], [11], or seven [12] parameter values, where a system of equations is derived for specific operating points provided in datasheets of commercial PV modules, such as short circuit, open circuit, and maximum power. However, at environmental conditions different from STC, those techniques can provide parameters with no physical significance. For example, in [10], it is considered that the value found for $R_s$ at STC is the same for any environmental condition. This oversimplification contradicts the physical and constructive characteristics of the solar cell as observed in [13]. In [3], the saturation currents of both diodes are considered to be equal, which differs from observations made in [14], where the higher saturation current in diode $d_2$ was considered, representing the physical characteristic of silicon solar cells.

Other disadvantage of these models, maybe the most important one, is that the parameters' identification is performed only at a specific temperature and irradiance (usually, the STC). Consequently, it is necessary to determine a completely different set of parameters for each environmental condition the model should represent. For example, in [15], the algorithm should be executed for all desired combinations of $S$ and $T$. As a result, those sets of parameters represent the best fitting for specific *I–V* curves, not depicting the physical phenomena of the PV cells.

In [2], an estimation technique was proposed to identify the parameters of the single-diode model that showed some correspondence with the physical behavior of the PV modules. The technique was based on a complete scan of the possible values of the parameters at the STC and considered only the dependence of $R_s$ with $T$ and $S$. Although interesting, the physical representation of this technique is limited, since it did not consider the dependence of other parameters with $T$ and $S$, i.e., it could not fully represent the physical phenomena of the PV modules. Other set of techniques use explicit equations [16] or optimization algorithms [17], [18] in order to build a quasi-adaptive model, i.e., they assume that some parameters, such as $R_s$ and $R_p$, do not depend on $T$ and $S$, although this simplification is not accurate [13], [14].

The adaptive models available in literature, that are based on the PV module's physics, can be divided in two categories: Online models based on simple explicit equations, where the parameters are translated when $T$ and $S$ shift from their reference values [19], [20], and offline models based on optimization algorithms, where the parameters' dependence with $T$ and $S$ are imposed by a set of physical equations, generating an extensive set of auxiliary parameters [21], [22]. The main advantage of the first category is that only the data available on datasheets and explicit equations are needed to build the complete model. This makes possible to embed both the parameter extraction and the full PV model in microcontrollers, i.e., the complete technique is online. On the other hand, the main disadvantage of those models is the poor representation of the real *P–V* curves of the module, reaching errors in power above 10% [19]. The main advantage of the second category is the high accuracy in representing the real *P–V* curves of the module, reaching errors in power below 1%. On the other hand, the parameter extraction technique based on optimization algorithms should be carried out offline, in a personal computer. After obtaining the parameters offline, it is possible to embed the full PV model in microcontrollers, similarly to the online techniques.

The difficulties and limitations encountered in the parameter estimation process of PV models have made the single-diode representation a bit more attractive than the double diode. However, even with a larger number of parameters and higher computational complexity, the double-diode model corresponds the physical behavior of solar generators more accurately, especially when it is important to define the efficiency of PV systems [23], justifying it as a research topic. In addition, there are only a few references that treat the parameters of the PV module in a broad approach, i.e., considering their relation with $S$ and $T$. The connection of the parameters of the model with the physical phenomena of PV modules covers areas of application, such as fault detection, reliability, and premature degradation diagnosis of the PV systems, very important for predictive and corrective maintenance.

The first contribution of this paper is the proposition of an irradiance and temperature dependent double-diode model for PV modules. In this model, the internal parameters depend on the environmental conditions, extrapolating its use for values of $T$ and $S$ different from those the parameters were initially estimated. In addition, two parameter estimation techniques are proposed for this new model. The techniques use a combination of analytical equations and numerical optimization based on the pattern search (PS) algorithm. Comparison results based on experimental *I–V* curves of real PV modules are presented in

order to prove the accuracy of the model and techniques when compared with other available works.

## II. Proposed Double-Diode Model

Based on the electric circuit of the double-diode model (see Fig. 1), the PV output current $I$ is given by

$$I = I_g - I_{01}\left[e^{\left(\frac{V+IR_s}{A_1V_t}\right)} - 1\right] - I_{02}\left[e^{\left(\frac{V+IR_s}{A_2V_t}\right)} - 1\right] - \frac{V+IR_s}{R_p} \quad (1)$$

where $V$ is the output voltage; $I_{01}$, $I_{02}$, $A_1$, and $A_2$ are the reverse saturation currents and the ideality factors that represent the diffusion and recombination phenomena, respectively; and $V_t$ is the thermal voltage given by

$$V_t = \frac{N_s k_B T}{q} \quad (2)$$

where $N_s$ is the number of series-connected cells in the PV module; $T$ is the temperature (K); $k_B$ is the Boltzmann constant ($k_B = 1.38 \times 10^{-23}$ J/K), and $q$ is the electron charge ($q = 1.6 \times 10^{-19}$ C).

Based on the $p-n$ junction theory [7] and the characteristics of the silicon cells [14], it is possible to relate the reverse saturation current for the diffusion phenomenon with the $T$ through

$$I_{01}(T) = I_{01,r}\left(\frac{T}{T_r}\right)^{3/A_1} e^{\left[\frac{q}{A_1k_B}\left(\frac{E_g(T_r)}{T_r} - \frac{E_g(T)}{T}\right)\right]} \quad (3)$$

where $I_{01,r}$ and $T_r$ are the saturation current and the temperature in the reference environmental condition. Moreover, it is important to notice that, like the reverse saturation current, the energy gap is also a function of $T$, defined as

$$E_g(T) = E_g(0) - \frac{aT^2}{T+b} \quad (4)$$

where $E_g(0)$ is the reference energy at 0 K, $a$ and $b$ are constants that depend on the material [24].

The studies carried out in this paper for several PV modules lead to the conclusion that $R_s$ and $R_p$ dependence with $S$ is defined by a power function and with $T$ is defined by a linear function. These dependencies are also in accordance with some results found in the literature [7], [13]. Based on this analysis, the expressions for $R_s$ and $R_p$ are defined as

$$R_s(S,T) = R_{s,T}\left[1 + k_{R_s}(T - T_r)\right] + R_{s,S}\left(\frac{S}{S_r}\right)^{-\gamma_{R_s}} \quad (5)$$

$$R_p(S,T) = R_{p,r}\left[1 - k_{R_p}(T - T_r)\right]\left(\frac{S}{S_r}\right)^{-\gamma_{R_p}} \quad (6)$$

where $R_{s,T}$, $R_{s,S}$, and $R_{p,r}$ are the dominant resistances for the reference environmental condition ($S_r$ and $T_r$); $k_{Rs}$ and $k_{Rp}$ are, respectively, the linear coefficients for $R_s$ and $R_p$ with respect to $T$; and $\gamma_{Rs}$ and $\gamma_{Rp}$ are, respectively, the exponential coefficients for $R_s$ and $R_p$ with respect to $S$.

For the photogenerated current, the analysis confirmed its proportional increase with $S$, along with the linear variation with $T$. Therefore, the following can be obtained:

$$I_g(S,T) = \left[I_{g,r} + \alpha_{I_{sc}}(T - T_r)\right]\left(\frac{S}{S_r}\right) \quad (7)$$

where $\alpha_{I_{sc}}$ is the linear coefficient for $I_{sc}$ with respect to $T$, defined by the datasheet of the PV module.

It is also important to determine the dependence of $V_{oc}$ with the environmental conditions, since it is related with the reverse saturation current for the recombination phenomenon $I_{02}$. Based on this analysis, it is possible to determine the logarithmic dependence of $V_{oc}$ with respect to $S$, along with the known linear variation with respect to $T$. Thus, it can be written as

$$V_{oc}(S,T) = V_{oc,r} + \beta_{V_{oc}}(T - T_r) + k_{V_{oc}}T\ln\left(\frac{S}{S_r}\right) \quad (8)$$

where $\beta_{V_{oc}}$ and $k_{V_{oc}}$ are the coefficients for $V_{oc}$ with respect to $T$ and $S$, respectively. $\beta_{V_{oc}}$ is defined by the datasheet of the PV module.

Based on the studies, the last two parameters, ideality factors $A_1$ and $A_2$, are constant, i.e., do not depend on $S$ and $T$. In Section III, two parameters' estimation techniques are proposed for this temperature and irradiance dependent double-diode model.

## III. Hybrid Pattern Search Estimation Techniques

In order to overcome the limitations of some techniques, associated with the availability of datasheet or experimental *P–V* curves with variable $S$ and fixed $T$ and fixed $S$ and variable $T$ conditions [2] and the necessity to carry out several curve fittings, this paper proposes two parameter estimation techniques based on the optimization algorithm known as PS, which tool is available on MATLAB. These proposed techniques use a hybrid approach for the parameter estimation, that is an association between the analytical calculation of some parameters and the determination of others through the PS optimization algorithm. Thus, these new techniques are called Hybrid PS (HPS) techniques.

The PS optimization algorithm is contained within a subset of direct search methods, i.e., they do not need information about the objective function's gradient. Direct search methods may well be used to solve noncontinuous, nondifferentiable, and multimodal optimization problems, with multiple local optima. In addition, the PS demonstrates good flexibility, simplicity of implementation, ease of application, minimum dependence on initial points in the final solution, and guarantee of global convergence [25]. Therefore, it is as a good candidate to deal with the problem of parameters estimation of the PV modules.

The HPS techniques are divided into two steps: Step 1—parameters estimation for the reference environmental condition; Step 2—estimation of the other parameters based on *I–V* and *P–V* curves with mixed values of $S$ and $T$. Two approaches of the parameters estimation for the reference environmental condition are proposed and they are called HPS1 and HPS2 techniques.

### A. Step 1—Reference Environmental Condition—HPS1

In the first step, the PS optimization algorithm is executed for the reference environmental condition, i.e., reference *I–V* or *P–V* curve. In order to build the optimization problem, it is necessary first to modify the analytical equations already presented to find some specific parameters.

Using the short-circuit condition $(V, I) = (0, I_{\text{sc}})$ in (1), it yields

$$I_{\text{sc}} = I_g - I_{01}\left[e^{\left(\frac{I_{\text{sc}}R_s}{A_1V_t}\right)} - 1\right] - I_{02}\left[e^{\left(\frac{I_{\text{sc}}R_s}{A_2V_t}\right)} - 1\right] - \frac{I_{\text{sc}}R_s}{R_p}. \tag{9}$$

Isolating the photogenerated current in (9), one has

$$I_g = I_{\text{sc}}\left(1 + \frac{R_s}{R_p}\right) + I_{01}\left[e^{\left(\frac{I_{\text{sc}}R_s}{A_1V_t}\right)} - 1\right] + I_{02}\left[e^{\left(\frac{I_{\text{sc}}R_s}{A_2V_t}\right)} - 1\right]. \tag{10}$$

The first parameter $I_g$ is calculated by the analytical (10) instead of (7). Thus, it is not necessary to determine the value of $I_{g,r}$. On the other hand, (10) depends on $I_{\text{sc}}$ that is given by

$$I_{\text{sc}}(S, T) = [I_{\text{sc},r} + \alpha_{I_{\text{sc}}}(T - T_r)]\left(\frac{S}{S_r}\right) \tag{11}$$

where $I_{\text{sc},r}$ is the point $(V, I) = (0, I_{\text{sc}})$ of the reference *I–V* curve and $\alpha_{I_{\text{sc}}}$ is given by the datasheet of the PV module. Similarly, in (8) $V_{\text{oc},r}$ is the point $(V, I) = (V_{\text{oc}}, 0)$ of the reference *I–V* curve.

The HPS1 technique first estimates the parameters for the reference environmental condition, $A_1$, $A_2$, $R_{s,r}$, $R_{p,r}$, and $I_{01,r}$, where

$$R_{s,T} + R_{s,S} = R_{s,r}. \tag{12}$$

However, after some simulations, it was noted that $I_{01,r}$ was mainly responsible for the lack of convergence of the PS algorithm, since its value is much smaller than other parameters, varying from $10^{-12}$ to $10^{-5}$. As an alternative solution, the expression

$$I_{01} = I_{02} \cdot 10^{-J} \tag{13}$$

is used, where $J_{\max} = 7$ [14]. Thus, $I_{01}$ is indirectly encountered by using (13).

Using $(V, I) = (V_{\text{oc}}, 0)$ (open-circuit condition) in (1), it yields

$$0 = I_g - I_{01}\left[e^{\left(\frac{V_{\text{oc}}}{A_1V_t}\right)} - 1\right] - I_{02}\left[e^{\left(\frac{V_{\text{oc}}}{A_2V_t}\right)} - 1\right] - \frac{V_{\text{oc}}}{R_p}. \tag{14}$$

In order to find the value of $I_{02}$, $I_g$ in (10) is substituted into (14), resulting in

$$I_{02} = \frac{I_{\text{sc}}\left(1 + \frac{R_s}{R_p}\right) - \frac{V_{\text{oc}}}{R_p} + I_{01}\left[e^{\left(\frac{I_{\text{sc}}R_s}{A_1V_t}\right)} - e^{\left(\frac{V_{\text{oc}}}{A_1V_t}\right)}\right]}{e^{\left(\frac{V_{\text{oc}}}{A_2V_t}\right)} - e^{\left(\frac{I_{\text{sc}}R_s}{A_2V_t}\right)}}. \tag{15}$$

Using (13) into (15) results in

$$I_{02} = \frac{10^J[I_{\text{sc}}(R_p + R_s) - V_{\text{oc}}]/R_p}{e^{\left(\frac{V_{\text{oc}}}{A_1V_t}\right)} - e^{\left(\frac{I_{\text{sc}}R_s}{A_1V_t}\right)} + 10^J\left[e^{\left(\frac{V_{\text{oc}}}{A_2V_t}\right)} - e^{\left(\frac{I_{\text{sc}}R_s}{A_2V_t}\right)}\right]}. \tag{16}$$

In this way, (10), (13), and (16) constitute the analytical equations of the HPS1 technique, which depend on the value of $I_{\text{sc}}$ given by (11). Thus, the PS algorithm is responsible to find the parameters $A_1$, $A_2$, $R_{s,r}$, $R_{p,r}$, and $J$, based on the minimization of a objective function: The value of mean absolute error in power (MAEP) between the reference *P–V* curve and the one generated by the model. The MAEP is defined by [2]

$$\text{MAEP} = \frac{\sum_{n=1}^{N_p} \text{error}_n}{N_p} \tag{17}$$

where $N_p$ is the number of voltage points extracted from the reference *P–V* curve and $\text{error}_n$ is the absolute error in power for the voltage point $n$, calculated by

$$\text{error} = |P_{\text{curve}} - P_{\text{model}}| \tag{18}$$

where $P_{\text{curve}}$ is the product of $V_{\text{curve}}$ and $I_{\text{curve}}$ obtained by the reference *P–V* curve and $P_{\text{model}}$ is the product of $V_{\text{model}}$ and $I_{\text{model}}$ obtained by solving (1).

In HPS1 algorithm, $X = [A_1; A_2; R_{s,r}; R_{p,r}; J]$ denotes the best vector, associated with the smallest value of MAEP. The vector $X$ is sought within the lower and upper limits, $\text{LL} = [1; 1; 0.1; 100; 0]$ and $\text{UL} = [2; 2; 2; \infty; 7]$. In order to define the best starting vector ($X_0 = [A_{1,0}; A_{2,0}; R_{s,0}; R_{p,0}; J_0]$), the value of MAEP is calculated for a limited number of possible starting vectors equally spaced among the lower and upper limits LL and UL. The chosen starting vector $X_0$ is the one that returns the lowest value of MAEP among all vectors evaluated. The stopping criteria of the PS algorithm are maximum number of iterations: 3000; maximum number of function evaluations: 100 000; mesh tolerance: $10^{-16}$; variable tolerance: $10^{-16}$; function tolerance: $10^{-16}$. After the optimization process, the parameters $A_1$, $A_2$, $R_{s,r}$, $R_{p,r}$, and $J$ are found and used in step 2 of the HPS1 technique.

### B. Step 1—Reference Environmental Condition—HPS2

An alternative that can be done in the optimization problem for step 1 is to use additional explicit equations to reduce the total number of parameters left in the search process of the optimization algorithm. In HPS2, the best choice for the optimization variables is $A_1$, $A_2$, $R_{s,r}$, $R_{p,r}$. In this case, (13) is not required. First, (10) is repeated here for clarity

$$I_g = I_{\text{sc}}\left(1 + \frac{R_s}{R_p}\right) + I_{01}\left[e^{\left(\frac{I_{\text{sc}}R_s}{A_1V_t}\right)} - 1\right] + I_{02}\left[e^{\left(\frac{I_{\text{sc}}R_s}{A_2V_t}\right)} - 1\right]. \tag{19}$$

The second and third terms in (19) are much smaller than $I_{\text{sc}}$, since the diodes are in short-circuit condition. Thus, the first term is the dominant term in (19) and an approximate equation

for $I_g$ can be written as

$$I_g = I_{sc}\left(1 + \frac{R_s}{R_p}\right). \tag{20}$$

Using $(V, I) = (V_{oc}, 0)$ (open-circuit condition) and $(V, I) = (V_{mp}, I_{mp})$ (MPP condition) in (1), it yields

$$0 = I_g - I_{01}\left[e^{\left(\frac{V_{oc}}{A_1 V_t}\right)} - 1\right] - I_{02}\left[e^{\left(\frac{V_{oc}}{A_2 V_t}\right)} - 1\right] - \frac{V_{oc}}{R_p} \tag{21}$$

$$I_{mp} = I_g - I_{01}\left[e^{\left(\frac{V_{mp}+I_{mp}R_s}{A_1 V_t}\right)} - 1\right] - I_{02}\left[e^{\left(\frac{V_{mp}+I_{mp}R_s}{A_2 V_t}\right)} - 1\right] - \left(\frac{V_{mp} + I_{mp}R_s}{R_p}\right). \tag{22}$$

Thus, by isolating $I_{02}$ in (21) and $I_{01}$ in (22), two coupled equations are obtained

$$I_{02} = \frac{I_g - \frac{V_{oc}}{R_p} - I_{01}\left[e^{\left(\frac{V_{oc}}{A_1 V_t}\right)} - 1\right]}{e^{\left(\frac{V_{oc}}{A_2 V_t}\right)} - 1} \tag{23}$$

$$I_{01} = \frac{I_g - I_{mp}\left(1 + \frac{R_s}{R_p}\right) - \frac{V_{mp}}{R_p} - I_{02}\left[e^{\left(\frac{V_{mp}+I_{mp}R_s}{A_2 V_t}\right)} - 1\right]}{e^{\left(\frac{V_{mp}+I_{mp}R_s}{A_1 V_t}\right)} - 1}. \tag{24}$$

However, substituting (23) into (24), $I_{01}$ can be written as

$$I_{01} = \frac{\left(\frac{V_{oc}}{R_p} - I_g\right)\left[\frac{e^{\left(\frac{V_{mp}+I_{mp}R_s}{A_2 V_t}\right)} - 1}{e^{\left(\frac{V_{oc}}{A_2 V_t}\right)} - 1}\right]}{\left[1 - e^{\left(\frac{V_{oc}}{A_1 V_t}\right)}\right]\frac{e^{\left(\frac{V_{mp}+I_{mp}R_s}{A_2 V_t}\right)} - 1}{e^{\left(\frac{V_{oc}}{A_2 V_t}\right)} - 1} + e^{\left(\frac{V_{mp}+I_{mp}R_s}{A_1 V_t}\right)} - 1} + \frac{I_g - \frac{V_{mp}}{R_p} - I_{mp}\left(1 + \frac{R_s}{R_p}\right)}{\left[1 - e^{\left(\frac{V_{oc}}{A_1 V_t}\right)}\right]\frac{e^{\left(\frac{V_{mp}+I_{mp}R_s}{A_2 V_t}\right)} - 1}{e^{\left(\frac{V_{oc}}{A_2 V_t}\right)} - 1} + e^{\left(\frac{V_{mp}+I_{mp}R_s}{A_1 V_t}\right)} - 1}. \tag{25}$$

In HPS2 algorithm, $I_g$ is calculated by (20), which depends on the value of $I_{sc}$ given by (11), $I_{02}$ by (23) and $I_{01}$ by (25). Note that the parameter *J* is absent in those new explicit equations. As consequence, $X = [A_1; A_2; R_{s,r}; R_{p,r}]$ denotes the best vector, associated with the smallest value of MAEP. The vector $X$ is sought within the lower and upper limits, $\mathrm{LL} = [1; 1; 0.1; 100]$ and $\mathrm{UL} = [2; 2; 2; \infty]$. In order to define the best starting vector ($X_0 = [A_{1,0}; A_{2,0}; R_{s,0}; R_{p,0}; J_0]$), the value of MAEP is calculated for a limited number of possible starting vectors equally spaced among the lower and upper limits LL and UL. The chosen starting vector $X_0$ is the one that returns the lowest value of MAEP among all vectors evaluated. After the optimization process, the parameters $A_1$, $A_2$, $R_{s,r}$, and $R_{p,r}$ are found and used in step 2 of the HPS2 technique.

### C. Step 2—Mixed Irradiance and Temperature Conditions

The second step is equal for both approaches (HPS1 and HPS2) of the first step. The second step has the purpose of determining the remaining parameters of the proposed double-diode model, $k_{V_{oc}}$ using curve fitting and $R_{s,S}$, $R_{s,T}$, $k_{R_s}$, $k_{R_p}$, $\gamma_{R_s}$, and $\gamma_{R_p}$ using the PS algorithm. In this step, (2), (5), (6), (8), (11), and (12) are used to build the optimization problem along with the parameters found in step 1. $I_g$, $I_{01}$, and $I_{02}$ are calculated by (10), (13), and (16) in HPS1 and by (20), (23), and (25) in HPS2. Additionally, datasheet or experimental *P–V* curves for different values of $S$ and $T$ should also be used. It is important to note that the proposed PV model is capable of representing the PV module in a wide range of $S$ and $T$ values only if the *P–V* curves used in step 2 have also a wide range of $S$ and $T$ values. The first part of this step is to obtain the points $(V, I) = (V_{oc}, 0)$ for every *I–V* curve and, using $\beta_{V_{oc}}$ from datasheet and $V_{oc,r}$ from the reference curve, to carry out a curve fitting in (8) in order to find $k_{V_{oc}}$. The second part is to execute the PS algorithm, seeking the minimization of the following objective function: The sum of MAEP of all *P–V* curves with different values of $S$ and $T$. The best vector $X = [R_{s,S}; k_{R_s}; k_{R_p}; \gamma_{R_s}; \gamma_{R_p}]$ is the one associated with the smallest value of the sum of MAEP. The vector $X$ is sought within the lower and upper limits, where $\mathrm{LL} = 10^{-5}$ has been defined for all parameters and $\mathrm{UL} = [R_{s,r}; 0.5; 0.5; 10; 10]$. The starting vector was defined by $X_0 = (\mathrm{UL} + \mathrm{LL})/2 + \mathrm{LL}$, which is the midpoint of the limits, and the stopping criteria are the same ones shown in Section IV-A, but with the maximum number of iterations extended to 5000, because of the higher complexity of step 2. It should be noted that $R_{s,T}$ is defined by (12) using the values of $R_{s,r}$ and $R_{s,S}$ found in steps 1 and 2, respectively. After the execution of these two steps, the complete set of parameters of the double-diode model is identified (see Fig. 2).

## IV. Experimental Results

Both HPS parameter estimation techniques for the proposed adaptive model are executed using the experimental *I–V* and *P–V* curves as inputs, obtained from a series of PV module measurements made by the National Renewable Energy Laboratory (NREL) that is publicly available.

### A. Curves Used for Parameter Estimation

The number of experimental *P–V* curves and the range of values of $S$ and $T$ are tested for the mSi0251 (polycrystalline silicon, located in Golden, CO, USA) to verify the accuracy of the parameter estimation techniques. The curves used in the parameter estimation have the irradiance and temperature in range $S = 210.0$–$1002.4$ W/m$^2$, $T = 24.8$–$51.0$ °C, respectively. These curves are presented in Table I, being classified as training and validation curves. The training curves are used in the parameter estimation process of the PV module following the steps 1 and 2 of Section III. The validation curves are used to test the extrapolation capability of the model obtained with the parameters estimated by the training curves. The curve number is related to the line of the original file available by NREL, such as

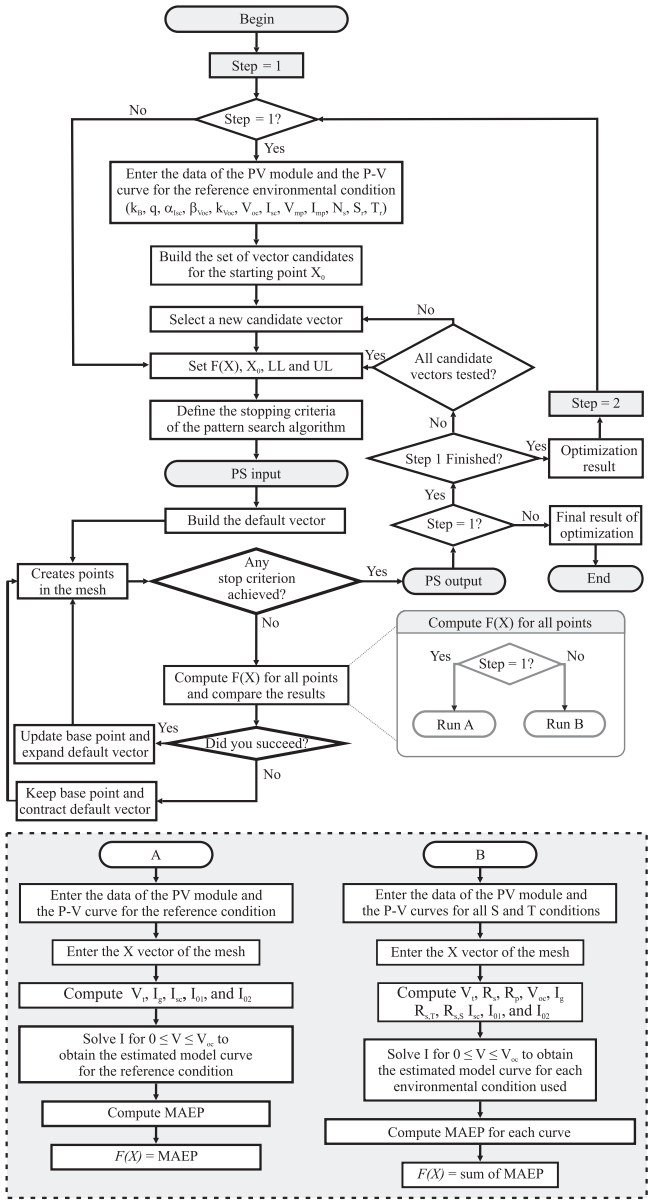


Fig. 2. Flowchart of the HPS techniques for double-diode model.

TABLE I
TRAINING AND VALIDATION CURVES USED IN THE PARAMETER ESTIMATION TECHNIQUES FOR PV MODULE mSi0251-Golden

| Curves | Number | S (W/m$^2$) | T ($^o$C) |
|---|---|---|---|
| Training | L37 | 709.1 | 51.0 |
| | L290 | 210.0 | 35.0 |
| | L444 | 812.4 | 48.4 |
| | L901 | 1002.4 | 45.9 |
| | L1268 | 306.8 | 24.8 |
| | L1367 | 598.8 | 44.2 |
| | L1650 | 404.2 | 27.2 |
| Validation | L16 | 701.8 | 46.7 |
| | L83 | 191.7 | 38.1 |
| | L731 | 128.8 | 31.1 |
| | L3135 | 601.1 | 28.0 |
| | L9370 | 1161.5 | 66.2 |

TABLE II
AVERAGE MAEP OF VALIDATION CURVES FOR DIFFERENT NUMBER OF TRAINING CURVES (PV MODULE mSi0251-Golden)

| Number of curves | Curves | $MAEP_a$ (W) |
|---|---|---|
| 3 | L444, L901, L1650 | 0.1439 |
| 4 | L444, L901, L1367, L1650 | 0.1547 |
| 5 | L290, L444, L901 L1367, L1650 | 0.1376 |
| 6 | L37, L290, L444 L901, L1367, L1650 | 0.1348 |
| 7 | L37, L290, L444, L901 L1268, L1367, L1650 | 0.1360 |

L37 means line 37 of the file mSi0251-Golden. It is important to mention that average uncertainties of the curves in Table I are given by: 2.4%, 1.9%, 0.325%, 0.2%, 0.358%, 0.258%, 0.375% for *S*, *T*, $I_{\rm sc}$, $V_{\rm oc}$, $I_{mp}$, $V_{mp}$, and $P_{mp}$, respectively. Many combinations of the curves in Table I are tested and the best results of MAEP$_a$ (average MAEP) of the validation curves used to test the extrapolation capability of the model are presented in Table II. The number of curves used to build the model are changed from three to seven and calculated the MAEP$_a$ for other five fixed curves with *S* and *T* conditions different from the training curves. It is possible to note that some curves have irradiance values (128.8 W/m$^2$) and temperature values (66.2 °C) outside the range of the training curves. It can be seen that all values of MAEP$_a$ are very low even for three training curves, proving the capability of the model to extrapolate other *S* and *T* conditions. Moreover, the small differences in MAEP$_a$ in Table II indicate that any number of training curves above three can be chosen. Five training curves is the number of curves used in all subsequent results in the paper.

### *B. Comparison Among Non-adaptive, Quasi-Adaptive, and Proposed Models*

A comparison among the proposed adaptive model with HPS parameter estimation techniques and other estimation techniques known in literature is carried out. In addition to MAEP, other evaluation metric is presented: Mean percentage error in power (MPEP), defined as

$$\text{MPEP} = \frac{\sum_{n=1}^{N_p} \text{error}_n\%}{N_p}. \tag{26}$$

The MAEP gives more importance to areas where the PV power is high (near the MPP) since the absolute differences between curves are higher in this region. The MPEP gives more importance to areas where the PV power is low (short circuit and open circuit) since the percentage differences between curves are higher in these regions (see Fig. 3) [2].

It is noteworthy that all model and techniques were executed using the same experimental *I–V* and *P–V* curves as inputs, obtained from NREL database. In the comparison tables, the techniques total scan for the single-diode model [2], proposed by Ishaque *et al.* [3] and proposed by Hejri *et al.* [10] are named as TS-1D, Ishaque, and Hejri. The proposed techniques based on PS are named as HPS1 and HPS2.

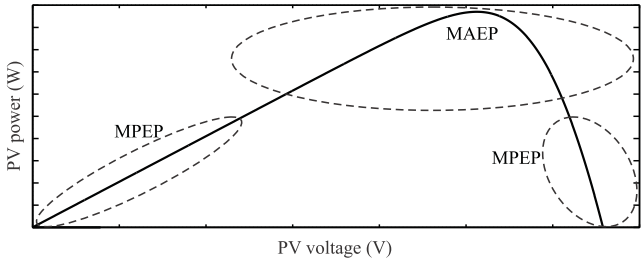


Fig. 3. Regions of MPEP and MAEP.

TABLE III
COMPARISON AMONG PROPOSED AND WELL-KNOWN PARAMETER ESTIMATION TECHNIQUES FOR PV MODULE mSi0251-Golden

| Parameters | TS-1D | Ishaque | Hejri | HPS1 | HPS2 |
|---|---|---|---|---|---|
| $A_1$ | 1.35 | 1 | 1 | 1 | 1.04 |
| $A_2$ | - | 2 | 2 | 1.76 | 1.92 |
| $R_{s,r}(\Omega)$ | 0.242 | 0.438 | 0.439 | 0.318 | 0.321 |
| $R_{s,S}(\Omega)$ | - | - | - | 0.0053 | 0.2533 |
| $R_{s,T}(\Omega)$ | - | - | - | 0.3125 | 0.068 |
| $R_{p,r}(\Omega)$ | 553.26 | 177.87 | 259.02 | 732.65 | 787.84 |
| $I_{g,r}$(A) | 2.686 | 2.686 | 2.691 | 2.687 | 2.687 |
| $I_{01,r}$(A) | $6.0{\cdot}10^{-7}$ | $2.9{\cdot}10^{-9}$ | $2.6{\cdot}10^{-9}$ | $1.8{\cdot}10^{-9}$ | $4.3{\cdot}10^{-9}$ |
| $I_{02,r}$(A) | - | $2.9{\cdot}10^{-9}$ | $7.1{\cdot}10^{-6}$ | $7.7{\cdot}10^{-6}$ | $1.5{\cdot}10^{-5}$ |
| J | - | - | - | 3.62 | - |
| $k_{R_s}(\%/^oC)$ | 15.6 | - | - | 1.08 | 4.69 |
| $k_{R_p}(\%/^oC)$ | - | - | - | 1.76 | 2.39 |
| $\gamma_{R_s}$ | $5.3{\cdot}10^{-6}$ | - | - | $1.0{\cdot}10^{-5}$ | $1.0{\cdot}10^{-5}$ |
| $\gamma_{R_p}$ | - | - | - | 0.283 | 0.280 |
| $V_{oc,r}$(V) | - | - | - | 20.4321 | 20.4321 |
| $k_{V_{oc}}(\%/^oC)$ | - | - | - | 0.35 | 0.35 |
| Comp. time (s) | 2.7 | 0.2 | 1.5 | 26.0 | 6.3 |
| $MAEP_r$ (W) | 0.032 | 0.396 | 0.231 | **0.018** | 0.019 |
| $MPEP_r$ (%) | 0.933 | 2.571 | 1.982 | **0.875** | 0.882 |
| $MAEP_a$ (W) | 0.169 | 0.332 | 0.235 | **0.066** | 0.066 |
| $MPEP_a$ (%) | 3.965 | 3.568 | 81.978 | **3.196** | 3.208 |

The bold values are used to highlight the best results for each figure of merit used for comparing the techniques.

The results in Table III correspond to the module mSi0251 (polycrystalline silicon, located in Golden, CO, USA) using training curves L290, L444, L901, L1367, and L1650 [see Table I, Fig. 4(a)]. The subscripts $r$ and $a$ in Table III refer to reference and average, respectively. In Table III, the parameters $A_1$, $A_2$, $R_{s,r}$, $R_{p,r}$, $I_{g,r}$, $I_{01,r}$, $I_{02,r}$, $J$, and $V_{\mathrm{oc},r}$ are calculated from the reference curve L901 (see Table I) and the parameters $R_{s,S}$, $R_{s,T}$, $k_{R_s}$, $k_{R_p}$, $\gamma_{R_s}$, and $\gamma_{R_p}$ are calculated from the training curves L290, L444, L901, L1367, and L1650 (see Table I). The validation curves L16, L83, L731, L3135, and L9370 in Fig. 4(b) (see Table I) confirm the extrapolation capability of the proposed model since the model curves match the experimental ones, i.e., the estimated parameters represent the PV module very well.

In Table III, it is possible to note that HPS1 technique presents the best results for all reference and average metrics. The graphical results for HPS2 are similar to HPS1 technique and, thus, they are omitted because of space limitation. It is important to mention that the proposed HPS1 technique has higher computation times than the other existing techniques. However, since the proposed techniques are executed offline (the parameter estimation process runs previously only one time), the computation time is not an essential figure of merit. It is more important to be accurate in the representation of the PV module, even if the computation time is higher. It is important to note that, after the estimation of the PV module parameters (offline), any characteristic *I–V* and *P–V* curves can be obtained executing the adaptive model with the desired values of *S* and *T*. This execution could be easily embedded in a microcontroller (online), since the adaptive model is simple, formed by explicit equations that depend only on *S* and *T*.

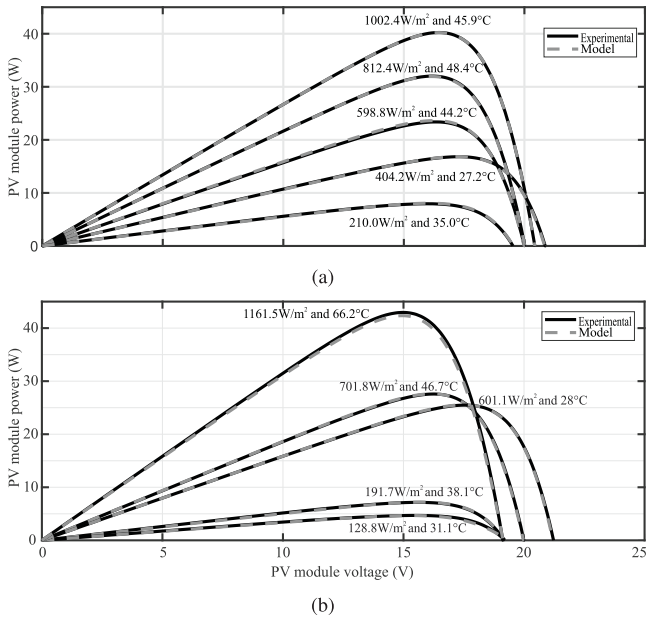


Fig. 4. Experimental and model curves obtained by the HPS1 technique for mSi0251-Golden. (a) Training curves to obtain the parameter estimation. (b) Validation curves to test the extrapolation capability of the model.

TABLE IV
COMPARISON AMONG PROPOSED AND WELL-KNOWN PARAMETER ESTIMATION TECHNIQUES FOR PV MODULE CdTe75638-Cocoa

| Parameters | TS-1D | Ishaque | Hejri | HPS1 | HPS2 |
|---|---|---|---|---|---|
| $A_1$ | 2 | 1 | - | 1 | 1 |
| $A_2$ | - | 2 | - | 2 | 2 |
| $R_{s,r}(\Omega)$ | 8.582 | 13.519 | - | 9.114 | 8.554 |
| $R_{s,S}(\Omega)$ | - | - | - | 0.228 | 8.5410 |
| $R_{s,T}(\Omega)$ | - | - | - | 8.886 | 0.0133 |
| $R_{p,r}(\Omega)$ | $1.2{\cdot}10^{3}$ | 801.55 | - | $1.6{\cdot}10^{3}$ | $1.4{\cdot}10^{3}$ |
| $I_{g,r}$(A) | 1.1508 | 1.1508 | - | 1.157 | 1.158 |
| $I_{01,r}$(A) | $1.0{\cdot}10^{-6}$ | $1.0{\cdot}10^{-12}$ | - | $9.4{\cdot}10^{-14}$ | $3.4{\cdot}10^{-15}$ |
| $I_{02,r}$(A) | - | $1.0{\cdot}10^{-12}$ | - | $9.4{\cdot}10^{-7}$ | $1.0{\cdot}10^{-6}$ |
| J | - | - | - | 7 | - |
| $k_{R_s}(\%/^oC)$ | 3.19 | - | - | 0.001 | 0.001 |
| $k_{R_p}(\%/^oC)$ | - | - | - | 0.031 | 0.001 |
| $\gamma_{R_s}$ | 0.3091 | - | - | 2.269 | 0.1426 |
| $\gamma_{R_p}$ | - | - | - | 0.4955 | 0.5640 |
| $V_{oc,r}$(V) | - | - | - | 86.2252 | 86.2252 |
| $k_{V_{oc}}(\%/^oC)$ | - | - | - | 1.12 | 1.12 |
| Comp. time (s) | 51.0 | 2.0 | - | 14.8 | 3.6 |
| $MAEP_r$ (W) | 0.1709 | 1.3903 | - | **0.1148** | 0.1324 |
| $MPEP_r$ (%) | 0.6923 | 4.9956 | - | **0.46** | 0.5281 |
| $MAEP_a$ (W) | 0.3673 | 1.2172 | - | **0.15** | 0.1616 |
| $MPEP_a$ (%) | 6.7623 | 8.4145 | - | **4.902** | 5.2130 |

The bold values are used to highlight the best results for each figure of merit used for comparing the techniques.

In order to verify the capability of the model to represent other technologies, the results in Table IV are presented for the module CdTe75638 (cadmium telluride, located at Cocoa, FL,

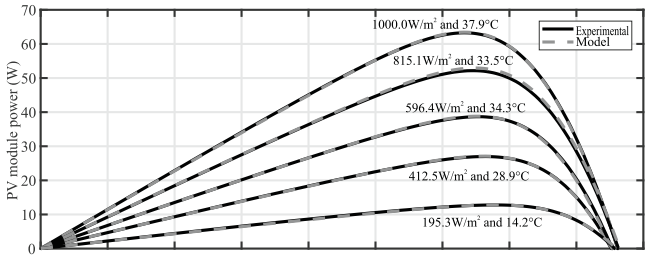


(a)

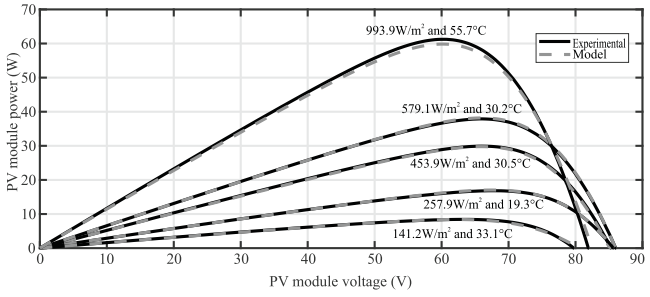


(b)

Fig. 5. Experimental and model curves obtained by the HPS1 technique for CdTe75638-Cocoa. (a) Training curves to obtain the parameter estimation. (b) Validation curves to test the extrapolation capability of the model.

TABLE V
COMPARISON AMONG ACTUAL AND ESTIMATED VALUES OF IMPORTANT OPERATION POINTS FOR PV MODULE mSi0251-GOLDEN

| Parameters | Actual | TS-1D | Ishaque | Hejri | HPS1 | HPS2 |
|---|---|---|---|---|---|---|
| $P_{mp}$ (W) | 40.235 | 40.242 | 40.221 | 40.227 | 40.258 | **40.235** |
| $V_{mp}$ (V) | 16.461 | 16.461 | 16.461 | 16.461 | 16.461 | **16.461** |
| $I_{mp}$ (A) | 2.444 | 2.445 | 2.443 | 2.444 | 2.446 | **2.444** |
| $V_{oc}$ (V) | 20.432 | 20.432 | 20.432 | 20.432 | 20.432 | **20.432** |
| $I_{sc}$ (A) | 2.688 | 2.685 | 2.679 | 2.686 | 2.686 | **2.686** |

The bold values are used to highlight the best results in terms of power, voltage and current among the techniques.

USA) using training curves L264 (412.5 W/m$^2$, 28.9 °C), L498 (815.1 W/m$^2$, 33.5 °C), L513 (1000.0 W/m$^2$, 37.9 °C), L587 (195.3 W/m$^2$, 14.2 °C) and L667 (596.4 W/m$^2$, 34.3 °C), shown in Fig. 5(a). In Table IV, the parameters $A_1$, $A_2$, $R_{s,r}$, $R_{p,r}$, $I_{g,r}$, $I_{01,r}$, $I_{02,r}$, $J$, and $V_{\mathrm{oc},r}$ are calculated from the reference curve L513 and the parameters $R_{s,S}$, $R_{s,T}$, $k_{R_s}$, $k_{R_p}$, $\gamma_{R_s}$, and $\gamma_{R_p}$ are calculated from the training curves L264, L498, L513, L587, and L667. The validation curves L262 (453.9 W/m$^2$, 30.5 °C), L799 (579.1 W/m$^2$, 30.2 °C), L1330 (257.9 W/m$^2$, 19.3 °C), L6628 (141.2 W/m$^2$, 33.1 °C) and L11139 (993.9 W/m$^2$, 55.7 °C) in Fig. 5(b) confirm the extrapolation capability of the proposed model since the model curves match the experimental ones, i.e., the estimated parameters represent the PV module very well. In Table IV, it is possible to note that HPS1 technique presents the best results for all reference and average metrics.

The important operation points $P_{mp}$, $V_{mp}$, $I_{mp}$, $V_{\mathrm{oc}}$, and $I_{\mathrm{sc}}$ for the proposed and existing techniques are shown in Table V for mSi0251-Golden and Table VI for CdTe75638-Cocoa. The actual values of the PV modules are obtained from NREL database. The reference curve of the module mSi0251-Golden has $S = 1002.4$ W/m$^2$, $T = 45.9$ °C, while the reference curve of the module CdTe75638-Cocoa has $S = 1000.0$ W/m$^2$, $T = 37.9$ °C.

TABLE VI
COMPARISON AMONG ACTUAL AND ESTIMATED VALUES OF IMPORTANT OPERATION POINTS FOR PV MODULE CdTe75638-Cocoa

| Parameters | Actual | TS-1D | Ishaque | Hejri | HPS1 | HPS2 |
|---|---|---|---|---|---|---|
| $P_{mp}$ (W) | 63.261 | 62.505 | 63.336 | - | 63.449 | **63.261** |
| $V_{mp}$ (V) | 63.223 | 63.711 | 63.711 | - | 63.223 | **63.223** |
| $I_{mp}$ (A) | 1.001 | 0.981 | 0.994 | - | 1.004 | **1.001** |
| $V_{oc}$ (V) | 86.225 | 86.225 | 86.225 | - | 86.225 | **86.225** |
| $I_{sc}$ (A) | 1.151 | 1.143 | 1.132 | - | 1.151 | **1.151** |

The bold values are used to highlight the best results in terms of power, voltage and current among the techniques.

TABLE VII
ESTIMATED VALUES OF IMPORTANT OPERATION POINTS AT STC FOR PV MODULE mSi0251-Golden (36 SERIES CELLS) AND CdTe75638-Cocoa (116 SERIES CELLS)

| Parameters | mSi0251-Golden | | CdTe75638-Cocoa | |
|---|---|---|---|---|
| | HPS1 | HPS2 | HPS1 | HPS2 |
| $P_{mp}$ (W) | 44.013 | 43.896 | 66.109 | 66.151 |
| $V_{mp}$ (V) | 18.043 | 18.043 | 65.964 | 65.964 |
| $I_{mp}$ (A) | 2.439 | 2.433 | 1.002 | 1.003 |
| $V_{oc}$ (V) | 21.953 | 21.953 | 88.934 | 88.934 |
| $I_{sc}$ (A) | 2.652 | 2.652 | 1.145 | 1.145 |

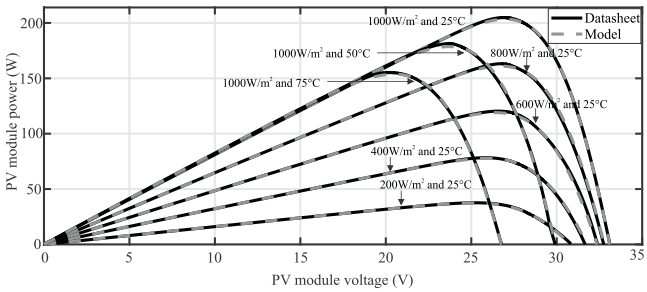


Fig. 6. Curves obtained by the HPS1 technique for the module KC200GT.

Hejri's technique does not present a positive value for $I_{01}$ in the module CdTe75638-Cocoa. Therefore, Hejri's technique is not considered adequate for this module (see Table VI). It can be seen that HPS2 technique obtained exactly the same values of $P_{mp}$, $V_{mp}$, $I_{mp}$, $V_{\mathrm{oc}}$, and $I_{\mathrm{sc}}$ for both PV modules, showing its accuracy also at important points of the *I–V* and *P–V* curves. The extrapolation capability of the HPS1 and HPS2 techniques is also used to estimate the $P_{mp}$, $V_{mp}$, $I_{mp}$, $V_{\mathrm{oc}}$, and $I_{\mathrm{sc}}$ values of both PV modules (mSi0251-Golden and CdTe75638-Cocoa) at STC, including the number of cell in series. These values are shown in Table VII.

### *C. Comparison Between Published and Proposed Adaptive Models*

A comparison between the proposed adaptive model with HPS1 parameter estimation technique and the adaptive model proposed in [22] with its parameter estimation technique is carried out to prove the high accuracy extrapolation capability of the proposed model. The *P–V* curves used in training and validation of the models are shown in Fig. 6 for the module KC200GT. This module is chosen for this last comparison because it is the same module used in [22]. The MAEP$_a$ of the seven curves in Fig. 6 for Mathew's technique [22] and proposed HPS1 technique are 0.550 and 0.342 W, respectively. From this result, is possible to

conclude that the proposed adaptive model with HPS1 technique represents the PV module KC200GT better.

## V. Conclusion

The environment-dependent double-diode model proposed in this paper can reproduce accurately the *I–V* and *P–V* behavior of real PV modules for irradiance and temperature conditions different from the ones used in the parameter estimation process. Because of this extrapolating capability, there is a wide range of applications for this model, such as the accurate estimation of the extracted power and energy of a PV power plant based on temperature and irradiance annual profiles of a specific place. However, the accuracy of a model depends on how precise the parameter estimation techniques can identify the real parameters of a PV module. Based on the experimental results, both proposed estimation techniques offer a reliable solution for PV model parameters estimation, fulfilling the requirement of high accuracy in all environmental conditions tested, even the conditions in which the parameters were not estimated. Besides that, the proposed double-diode model preserves the physical behavior of the PV module and offers a solution to the limitations found in other fixed models and their estimation techniques.

## References


[1] P. Wolf and V. Benda, "Identification of PV solar cells and modules parameters by combining statistical and analytical methods," *Sol. Energy*, vol. 93, pp. 151–157, 2013.

[2] E. A. Silva, F. Bradaschia, M. C. Cavalcanti, and A. J. Nascimento, Jr., "Parameter estimation method to improve the accuracy of photovoltaic electrical model," *IEEE J. Photovolt.*, vol. 6, no. 1, pp. 278–285, Jan. 2016.

[3] K. Ishaque, Z. Salam, and H. Taheri, "Simple, fast and accurate two-diode model for photovoltaic modules," *Sol. Energy Mater. Sol. Cells*, vol. 95, no. 2, pp. 586–594, 2011.

[4] Y. Mahmoud, W. Xiao, and H. H. Zeineldin, "A simple approach to modeling and simulation of photovoltaic modules," *IEEE Trans. Sustain. Energy*, vol. 3, no. 1, pp. 185–186, Jan. 2012.

[5] D. Rekioua and E. Matagne, *Optimization of Photovoltaic Power Systems: Modelization, Simulation and Control* (Green Energy and Technology), 1st ed. London, U.K.: Springer-Verlag, 2012.

[6] W. Xiao, W. G. Dunford, and A. Capel, "A novel modeling method for photovoltaic cells," in *Proc. IEEE 35th Annu. Power Electron. Specialists Conf.*, Jun. 2004, pp. 1950–1956.

[7] C.-T. Sah, R. N. Noyce, and W. Shockley, "Carrier generation and recombination in P-N junctions and P-N junction characteristics," *Proc. IRE*, vol. 45, no. 9, pp. 1228–1243, Sep. 1957.

[8] B. C. Babu and S. Gurjar, "A novel simplified two-diode model of photovoltaic (PV) module," *IEEE J. Photovolt.*, vol. 4, no. 4, pp. 1156–1161, Jul. 2014.

[9] S. Shongwe and M. Hanif, "Comparative analysis of different single-diode PV modeling methods," *IEEE J. Photovolt.*, vol. 5, no. 3, pp. 938–946, May 2015.

[10] M. Hejri, H. Mokhtari, M. R. Azizian, M. Ghandhari, and L. Soder, "On the parameter extraction of a five-parameter double-diode model of photovoltaic cells and modules," *IEEE J. Photovolt.*, vol. 4, no. 3, pp. 915–923, May 2014.

[11] E. I. Batzelis and S. A. Papathanassiou, "A method for the analytical extraction of the single-diode PV model parameters," *IEEE Trans. Sustain. Energy*, vol. 7, no. 2, pp. 504–512, Apr. 2016.

[12] A. A. Elbaset, H. Ali, and M. A.-E. Sattar, "Novel seven-parameter model for photovoltaic modules," *Sol. Energy Mater. Sol. Cells*, vol. 130, pp. 442–455, 2014.

[13] J. D. Arora, A. V. Verma, and M. Bhatnagar, "Variation of series resistance with temperature and illumination level in diffused junction poly- and single-crystalline silicon solar cells," *J. Mater. Sci. Lett.*, vol. 5, no. 12, pp. 1210–1212, 1986.

[14] M. Wolf, G. T. Noel, and R. J. Stirn, "Investigation of the double exponential in the current–voltage characteristics of silicon solar cells," *IEEE Trans. Electron Devices*, vol. 24, no. 4, pp. 419–428, Apr. 1977.

[15] D. F. Alam, D. A. Yousri, and M. B. Eteiba, "Flower pollination algorithm based solar PV parameter estimation," *Energy Convers. Manage.*, vol. 101, pp. 410–422, 2015.

[16] P.-H. Huang, W. Xiao, J. C.-H. Peng, and J. L. Kirtley, "Comprehensive parameterization of solar cell: Improved accuracy with simulation efficiency," *IEEE Trans. Ind. Electron.*, vol. 63, no. 3, pp. 1549–1560, Mar. 2016.

[17] P. Bharadwaj, K. N. Chaudhury, and V. John, "Sequential optimization for PV panel parameter estimation," *IEEE J. Photovolt.*, vol. 6, no. 5, pp. 1261–1268, Sep. 2016.

[18] A. I. Aldaoudeyeh, "Development of a generalised PV model in MATLAB/Simulink using datasheet values," *J. Eng.*, vol. 2018, no. 5, pp. 257–263, 2018.

[19] M. Hejri and H. Mokhtari, "On the comprehensive parametrization of the photovoltaic (PV) cells and modules," *IEEE J. Photovolt.*, vol. 7, no. 1, pp. 250–258, Jan. 2017.

[20] M. C. D. Piazza, M. Luna, G. Petrone, and G. Spagnuolo, "Translation of the single-diode PV model parameters identified by using explicit formulas," *IEEE J. Photovolt.*, vol. 7, no. 4, pp. 1009–1016, Jul. 2017.

[21] E. A. Silva *et al.*, "An eight-parameter adaptive model for the single diode equivalent circuit based on the photovoltaic module's physics," *IEEE J. Photovolt.*, vol. 7, no. 4, pp. 1115–1123, Jul. 2017.

[22] D. Mathew *et al.*, "Wind-driven optimization technique for estimation of solar photovoltaic parameters," *IEEE J. Photovolt.*, vol. 8, no. 1, pp. 248–256, Jan. 2018.

[23] A. M. S. Furtado, F. Bradaschia, M. C. Cavalcanti, and L. R. Limongi, "A reduced voltage range global maximum power point tracking algorithm for photovoltaic systems under partial shading conditions," *IEEE Trans. Ind. Electron.*, vol. 65, no. 4, pp. 3252–3262, Apr. 2018.

[24] P. Singh and N. Ravindra, "Temperature dependence of solar cell performance—An analysis," *Sol. Energy Mater. Sol. Cells*, vol. 101, pp. 36–45, 2012.

[25] S. T. Kebir, M. Haddadi, and M. S. Ait-Cheikh, "An overview of solar cells parameters extraction methods," in *Proc. 3rd Int. Conf. Control, Eng. Inf. Technol.*, May 2015, pp. 1–7.


**Fabricio Bradaschia** (S'10–M'13–SM'19) was born in Sao Paulo, Brazil, in 1983. He received the B.Sc., M.Sc., and Ph.D. degrees in electrical engineering from the Federal University of Pernambuco, Recife, Brazil, in 2006, 2008, and 2012, respectively.

From August 2008 to August 2009, he worked as a Visiting Scholar with the University of Alcala, Madrid, Spain. Since October 2013, he has been working as an Associate Professor with the Department of Electrical Engineering at the Federal University of Pernambuco. His research interests include application of power electronics in photovoltaic systems and power quality, including pulsewidth modulation, converter topologies, and grid synchronization methods.

**Marcelo C. Cavalcanti** was born in Recife, Brazil, in 1972. He received the B.Sc. degree in electrical engineering from the Federal University of Pernambuco, Recife, Brazil, in 1997, and the M.Sc. and the Ph.D. degrees in electrical engineering from the Federal University of Campina Grande, Campina Grande, Brazil, in 1999 and 2003, respectively.

From October 2001 to August 2002, he was a Visiting Scholar with the Center for Power Electronics Systems, Virginia Polytechnic Institute and State University, Blacksburg, VA, USA, and with University of Alcalá, Madrid, Spain, from September 2012 to August 2013. Since 2003, he has been with the Department of Electrical Engineering, Federal University of Pernambuco, where he is currently a Professor in electrical engineering. His research interests include applications of power electronics in renewable energy systems and power quality.

**Aguinaldo José do Nascimento, Jr.** was born in Recife, Brazil, in 1986. He received the B.Sc. and the M.Sc. degrees in physics and the Ph.D. degree in electrical engineering, all from the Federal Rural University of Pernambuco, Recife, Brazil, in 2010, 2014, and 2018, respectively.

His research interests include modeling and maximum power point tracking of photovoltaic systems.

**Emerson Alves da Silva** was born in Jaboatão dos Guararapes, Brazil, in 1990. He received the B.Sc., M.Sc., and Ph.D. degrees in electrical engineering from the University of Pernambuco, Recife, Brazil, in 2012, 2015, and 2019, respectively.

His research interests include modeling and maximum power point tracking of photovoltaic systems.

**Gustavo Medeiros de Souza Azevedo** (S'10–M'12) was born in Belo Jardim, Brazil, in 1981. He received the B.Sc., M.Sc., and the Ph.D. degrees in electrical engineering from the Federal University of Pernambuco, Recife, Brazil, in 2005, 2007, and 2011, respectively.

He worked as a Visiting Scholar with the Polytechnical University of Catalunya, Barcelona, Spain, from 2008 to 2009. Since 2014, he has been working as an Associate Professor with the Department of Electrical Engineering at the Federal University of Pernambuco. His research interests include renewable energy systems and microgrids.